

Long-range electromagnetic propagation above a polluted sea surface: hybrid modeling

Thomas Bonnafont, Ali Khenchaf

▶ To cite this version:

Thomas Bonnafont, Ali Khenchaf. Long-range electromagnetic propagation above a polluted sea surface: hybrid modeling. IEEE Geoscience and Remote Sensing Letters, 2024, pp.1-1. 10.1109/LGRS.2024.3447828. hal-04680816

HAL Id: hal-04680816 https://ensta-bretagne.hal.science/hal-04680816v1

Submitted on 12 Sep 2024

HAL is a multi-disciplinary open access archive for the deposit and dissemination of scientific research documents, whether they are published or not. The documents may come from teaching and research institutions in France or abroad, or from public or private research centers.

L'archive ouverte pluridisciplinaire **HAL**, est destinée au dépôt et à la diffusion de documents scientifiques de niveau recherche, publiés ou non, émanant des établissements d'enseignement et de recherche français ou étrangers, des laboratoires publics ou privés.

Long-range electromagnetic propagation above a polluted sea surface: hybrid modeling

Thomas Bonnafont, Ali Khenchaf Senior Member, IEEE,

Abstract

Modeling electromagnetic propagation in the maritime environment is a key element in calibrating detection tools, for example in SAR imaging. This article presents a method to compute the propagation above a polluted sea surface. The latter is based on the parabolic wave equation solved with the split-step wavelet method. A hybrid method is also used to account for the sea surface. Indeed, here the sea spectrum is used to both generate random sea surfaces and compute a roughness parameter. The contributions of this article are twofold. First, we improve the calculation of the roughness coefficient in the hybrid method by accounting for the shadowing effect. Second, a stochastic strategy is developed to account for an insoluble oil slick, or pollutant, that covers part of the domain. Numerical tests in the S-band are provided to validate the method and highlight its advantages.

Index Terms

electromagnetic propagation, parabolic wave equation, split-step, sea spectrum, pollution.

I. INTRODUCTION

Modeling electromagnetic propagation in the maritime environment is an essential step for detection, surveillance, and communication applications. In particular, if a pollutant is present then the geometrical and electromagnetic properties of the sea are changed [1], leading to a change of the received electromagnetic field that can be used to detect oil slicks [2]–[4]. The latter is useful, for example, to close fishing areas when needed and find polluting boats.

In this article, we focus on modeling the long-range propagation of electromagnetic waves over a polluted sea surface, assuming the pollutant is insoluble. This is a key element to calibrate the detection tools.

So far, the literature has mainly focused on computing the radar cross section (RCS) of the sea surface in a clean or polluted state [5]–[7]. They study the case of mono-static or bi-static back-scattering measurement, with a focus on the case of SAR imaging. In practice, they account for the sea surface through the sea spectrum [8], or its damped version in case of a polluted sea [1]. The latter is introduced into the electromagnetic field's integral equation and allows computing and comparing the RCS for the sea with and without an oil film. The difference between both has been utilized for detection purposes [7]. Some works [9] also modeled the sea geometry by generating random surfaces and accounted for the pollutant/sea interaction as a layered media.

Nonetheless, these works do not account for the refraction phenomena, despite evaporation ducts being common in the maritime environment. In [10], they propose to model the long-range forward propagation above a polluted sea surface, assuming a flat sea surface. A roughness coefficient computed with the sea spectrum has been introduced to model the effect of the sea. They show that detection is feasible, by comparing the field received at a given distance of the transmitter when the sea is polluted or not. Nonetheless, the refraction and the sea waves have not been accounted for. In addition, they only modeled a fully covered sea.

Another strand of the literature has focused more on accurately modeling the maritime long-range forward propagation [11], [12]. This is the case if we study the propagation from a coastal radar toward a receptor for example. In this case, the parabolic wave equation (PWE) [13] model is widely used since it allows accounting for the refraction, the relief, and the ground composition. Furthermore, with this model, the effect of the sea can accurately be accounted for through a hybrid approach [11], [12]. Indeed, sea surfaces are randomly generated to account for the effect of the waves.

In this article, we improve the hybrid approach from [11], by introducing a shadowed roughness coefficient as in [10]. Then, we apply it to model forward propagation over a polluted sea surface using the PWE. Furthermore, we consider both known and unknown positions of the oil film, using a stochastic model for the latter. Numerical experiments in the S-band validate the method, demonstrating feasible detection within a certain range.

II. THE PROPAGATION MODEL

This section derives the propagation model over clean and polluted sea surfaces. An $\exp(j\omega_0 t)$ time variation of the field, with ω_0 the angular frequency, is assumed. We use the Cartesian coordinates system (x, z), with x as the propagation direction.

Thomas Bonnafont and Ali Khenchaf are with Lab-STICC, UMR CNRS 6285, ENSTA Bretagne, Brest, France (email: thomas.bonnafont@ensta-bretagne.fr; ali.khenchaf@ensta-bretagne.fr)

A. The forward parabolic wave equation

The main goal is to compute the field received by a receptor at a given distance from the transmitter. Assuming a slowly varying refractive index n along x, we use the parabolic wave equation (PWE) [13], which reduces the mesh size limit along the propagation direction by considering only forward propagation in a paraxial cone. Denoting u as the reduced field [13], the wide-angle PWE is written as follows:

$$\frac{\partial u}{\partial x} = -j \left(\sqrt{\frac{\partial^2}{\partial z^2} + k_0^2} - k_0 \right) - jk_0(n-1)u, \tag{1}$$

where k_0 is the free-space wave number.

B. Modeling the sea effects

One of the key components to generate sea surfaces is the sea spectrum, which statistically describes the state of the sea for a given wind speed. Here, we use the widely employed Elfouhaily spectrum [8], denoted by S_{clean} , expressed as

$$S_{\text{clean}}(U_{10}, k) = \frac{1}{k^3} \left(S_{\text{low}}(U_{10}, k) + S_{\text{high}}(U_{10}, k) \right), \tag{2}$$

with k the wave number, and where $S_{\rm low}$ and $S_{\rm high}$, correspond to the long and short wave curvatures, respectively. The main variable for these parameters is the wind speed at 10 m above the sea [8], which hereafter is denoted by U_{10} . Examples of sea spectrum for different wind speeds can be found in [8], [11]. In general, $S_{\rm clean}$ also depends on the fetch, but here we assume a fully developed sea and omit this parameter for concision, but all can be directly extended to this case.

Then, since the spectrum describes the statistical properties of the sea state, it is used to generate sea surfaces $z_{\rm mer}$, which are described as random processes. This computation is performed in two steps. First, random geometries, denoted by $z_{\mathcal{N}}$, are generated following a standard normal distribution¹. Second, a convolution with $\sqrt{S_{\rm clean}}$ is performed to introduce the sea state properties. For computational efficiency, the latter is performed as follows [11]

$$z_{\text{mer}} = \mathcal{F}^{-1} \left(\sqrt{S_{\text{clean}}} \mathcal{F} \left(z_{\mathcal{N}} \right) \right), \tag{3}$$

with \mathcal{F} the Fourier transform. It should be emphasized that $z_{\rm mer}$ is a stochastic process that describes a sea state. Thus, only examples of realizations can be computed, and statistical strategies (such as Monte Carlo simulations) are needed to consider the sea effect. Examples of sea surface generation can be found in [11]

C. Introducing the pollutant

In this part, the effect of the pollutant is introduced, following Lombardini's model [1]. Indeed, we assume a wind speed lower than 8-10 m/s, where the oil is insoluble [1], [10].

To obtain the polluted sea spectrum, S_{po} , the usual damping model for partially covered sea [1], [5] is used leading to

$$S_{\text{po}} = S_{\text{clean}}(\mu U_{10}, k) \left(1 - F_{\text{po}} + F_{\text{po}}/y_{\text{damp}}\right),$$
 (4)

where $F_{\rm po}$ is the ratio of area covered by the pollutant, that changes the global structure of the surface, $\mu \in [0,1]$ a reduction factor accounting for reduced frictions on a slick covered sea [14], and $y_{\rm damp}$ is the damping ratio. The latter accounts for the attenuation due to the oil film and is written as

$$y_{\text{damp}}(k) = \frac{1 - 2\tau + 2\tau^2 - X + Y(X + \tau)}{1 - 2\tau + 2\tau^2 - 2X + 2X^2},$$
(5)

with $X(k)=\frac{E_0k^2}{\rho\sqrt{2\nu\omega^3}}, Y(k)=\frac{E_0k}{4\rho\nu\omega}, \tau(k)=\sqrt{\frac{\omega_{\rm po}}{2\omega}},$ and, $\omega(k)=\sqrt{\sigma k^3/\rho+gk}$, ρ the density of the sea water, $\omega_{\rm po}$ corresponds to the characteristic pulsation of the considered pollutant, E_0 to the oil's elasticity modulus, σ to the surface tension due the oil film, ν to the kinetic velocity, and g to the acceleration of gravity. We set $\mu=1$ since for $U_{10}\leq 8$ m/s empirical studies show that the wind speed has almost no effect on the oil slick [15], and to be in the worst-case scenario for detection. For more information on this model and the effect of each parameter, the interested reader is referred to [1], [10].

Now, one can wonder, what happens when $F_{\rm po} \neq 1$. In this case, there are two possibilities: either we know where the pollutant is or not. In the first case, the modeling is quite easy, since the damping model generates the sea surface. Then, the electromagnetic characteristics of the pollutant, $\varepsilon_{r,\rm po}$ and $\sigma_{\rm po}$, are used where the oil leak is present. Note that the presence of oil affects the whole considered sea surface.

In the other case, which is more interesting for detection, we propose to add another stochastic layer. Indeed, the position of the pollutant is now considered a random process. We assume a continuous oil slick for better readability, even if the proposed approach can be generalized to discontinuous ones. First, for a given F, the position of the oil leakage follows a uniform law

¹This can be interpreted as a Karhunen-Loeve expansion of the roughness, where the surface is computed as a sum of normal distribution.

 $x_{\rm po} \sim \mathcal{U}([0, (1-F_{\rm po})x_{\rm max}])$, with $x_{\rm max}$ the total size. Thus, the position of the pollutant $x_{\rm po}$ can be easily generated. In $[x_{\rm po}, x_{\rm po} + F_{\rm po}x_{\rm max}]$, the ground parameters correspond to the oil's dielectric parameters, while the rest of the area is seawater. Second, the polluted sea spectrum is computed to generate random polluted sea surfaces. Note that for one position the mean of the propagated field needs to be computed. On the contrary, to see the effect of the position of the pollutant on the field and the detection ability, no mean over the different $x_{\rm po}$ is calculated.

Note that if an emulsion of water and oil is considered a mixing formula [9] for ε and σ can be used. Finally, a composite layered medium model [9] could also be used, and the method developed hereafter can be generalized to this case.

III. THE COMPUTATIONAL METHOD

A. The computational domain

The computational domain Ω is of sizes x_{\max} and z_{\max} along the horizontal and vertical axis, respectively. We assume the field to be known at x=0, with the source placed at $x_{\rm s} \leq 0$. We are interested in the propagation above the ground, leading to $\Omega = [0, x_{\max}] \times [0, z_{\max}]$.

For numerical reasons, Ω is discretized along x and z, with N_x and N_z corresponding to the number of points. The mesh sizes along both directions are thus given by $\Delta x = x_{\rm max}/N_x$, and $\Delta z = z_{\rm max}/N_z$. We denote by $u_{\rm x}[\cdot]$ the field at the position x discretized along z.

Nonetheless the discretization along the propagation direction x introduces a cut-off to the sea spectrum [11], [12]. Thus, only the lowest part of the latter, until $k_{\text{max}} = N_x 2\pi/x_{\text{max}}$, can be used to generate representative random sea surfaces.

B. Split-step wavelet

This section gives a brief overview of the split-step wavelet (SSW) method [16] used here to solve equation (1).

With SSW the field is computed iteratively along x in two steps. First, the field is propagated in a layer of free space from x to $x + \Delta x$ in the wavelet domain. Second, the effects of the refraction, the relief, and the ground composition are considered in the spatial domain. This can be summarized as

$$u_{x+\Delta x} = RLW^{-1}PC_{V_f}Wu_x, \tag{6}$$

where W corresponds to the wavelet transform, C_{V_f} to a hard-threshold compression (all the coefficients below V_f are set to 0) applied to the field wavelet coefficients, P to the sparse wavelet-to-wavelet scattering operator [16], and R and L operators accounting for the relief and the refraction in the spatial domain. The phase-screen method is used for the latter [13], while a staircase model is used for the relief. Note that with SSW, one can consider the refraction – such as surface duct – in the model, differentiating from other previous works such as [10]. The local image method [17] is used to account for the ground composition. As for the image theorem, the ground parameters are accounted for via the Fresnel coefficient Γ_0 , but using fewer points.

The SSW method is used here because of its efficiency in both computation time and memory usage [16], which is important for the Monte Carlo simulations.

C. The shadowed hybrid approach

As said before, the lowest part of the spectrum, i.e., $k \le k_{\text{max}}$, is used to generate random sea surfaces. For the highest part, $k \ge k_{\text{max}}$, of the spectrum that models the capillary waves, we introduce a roughness coefficient [11], denoted by ρ_{h} , that allows taking their effects as an attenuation. It can be computed using either the Ament [18] or the Miller-Brown formula [19]. Hereafter, we use the Ament one given by

$$\rho_{\rm h} = \exp\left(-\gamma^2/2\right),\tag{7}$$

where $\gamma = 2k_0h_s\sin(\theta_g)$, θ_g the grazing angle and h_s the surface RMS height. Here, since the roughness coefficient is computed with the highest part of the sea spectrum, the surface RMS height of the capillary waves is calculated as follows

$$h_s = \sqrt{\int_{k_{max}}^{+\infty} S(k)dk},\tag{8}$$

where S is either the clean or polluted sea spectrum. The new reflection coefficient Γ is then obtained as $\Gamma = \rho_h \Gamma_0$.

Nonetheless, this coefficient does not account for the shadowing effect of capillary waves, which is important when the entire spectrum is used [20]. Therefore, we propose a new roughness coefficient, $\rho_h^{\rm sh}$, that includes this shadowing effect. This new coefficient replaces ρ_h in the previous method. Following [20], we use the Smith formulation for more accurate results, leading to the following integral computation:

$$\rho_{\rm h}^{\rm sh} = \int_{-\infty}^{+\infty} e^{2jk_0\zeta \sin\theta_g} p_{\zeta}(\zeta) (1+2\Lambda) \left(F(\zeta)\right)^{2\Lambda} d\zeta, \tag{9}$$

with p_{ζ} the probability density function for the height ζ , corresponding to Gaussian statistics in the case of the Ament coefficient [18]. The integral in equation (9) also depends on Λ and F that are defined in the Smith formulation as

$$\Lambda(v) = \frac{\exp(-v^2) - v\sqrt{\pi}\operatorname{erfc}(v)}{2v\sqrt{\pi}},
F(\zeta) = 1 - \frac{1}{2}\operatorname{erfc}\left(\frac{\zeta}{\sqrt{2}h_s}\right), \tag{10}$$

with $v = \frac{\tan \theta_g}{\sqrt{2}\sigma_{\sigma}}$, and σ_{γ} the RMS slope. Using the highest part of the Elfouhaily spectrum, the latter is computed as

$$\begin{aligned}
\sigma_{\gamma} &= \alpha_{\gamma} + \beta_{\gamma} \\
\alpha_{\gamma} &= \int_{k_{\text{max}}}^{+\infty} \frac{1}{k} \left(S_{\text{low}} \left(U_{10}, k \right) + S_{\text{high}} \left(U_{10}, k \right) \right) dk \\
\beta_{\gamma} &= \int_{k_{\text{max}}}^{+\infty} \frac{1}{k} \left(S_{\text{low}} \left(U_{10}, k \right) + S_{\text{high}} \left(U_{10}, k \right) \right) \Delta(k) dk
\end{aligned}$$

where $\Delta(k)$ corresponds to the Elfouhaily spreading function [8]. After computing all these parameters, a numerical quadrature is needed to compute the shadowed roughness coefficient, leading to an increase in the computation time. Nonetheless, using a Gaussian fitting, one can approximate this integral [10], [20], [21]. Since SSW has a very low complexity we opt for the numerical quadrature for a better accuracy here.

IV. NUMERICAL TESTS

All tests are performed at $f_0=3$ GHz (S-band) in $\Omega=[0,5000]\times[0,128]$ m 2 . For the discretization, we use: $\Delta x=100\lambda=10$ m and $\Delta z=\lambda/2=0.05$ m, ensuring good accuracy with the PWE model. A complex source point [22] at $x_s=-50$ m and $z_s=20$ m models the antenna, with a width of 3 m. The ground is modeled as either seawater ($\varepsilon_r=80,\sigma=5$ S/m) or petrol ($\varepsilon_{r,\mathrm{po}}=2.2,\sigma_{\mathrm{po}}=0.0017$ S/m) if polluted [23]. An atmospheric surface duct is also considered, a common phenomenon above the sea.

A. Comparison of the roughness coefficients

In this first numerical experiment, we consider the case of a clean sea with a wind speed $U_{10} = 10$ m/s.

We consider the propagation over a flat sea using the Ament coefficient, and the hybrid model with or without the shadowed coefficient. A Monte Carlo study with 50 samples is performed for the last two, to estimate the mean and the standard deviation. In Fig. 1, we plot the field in dB computed at the last iteration in each case. For the hybrid approaches, we plot the mean and the 99% confidence interval (CI).

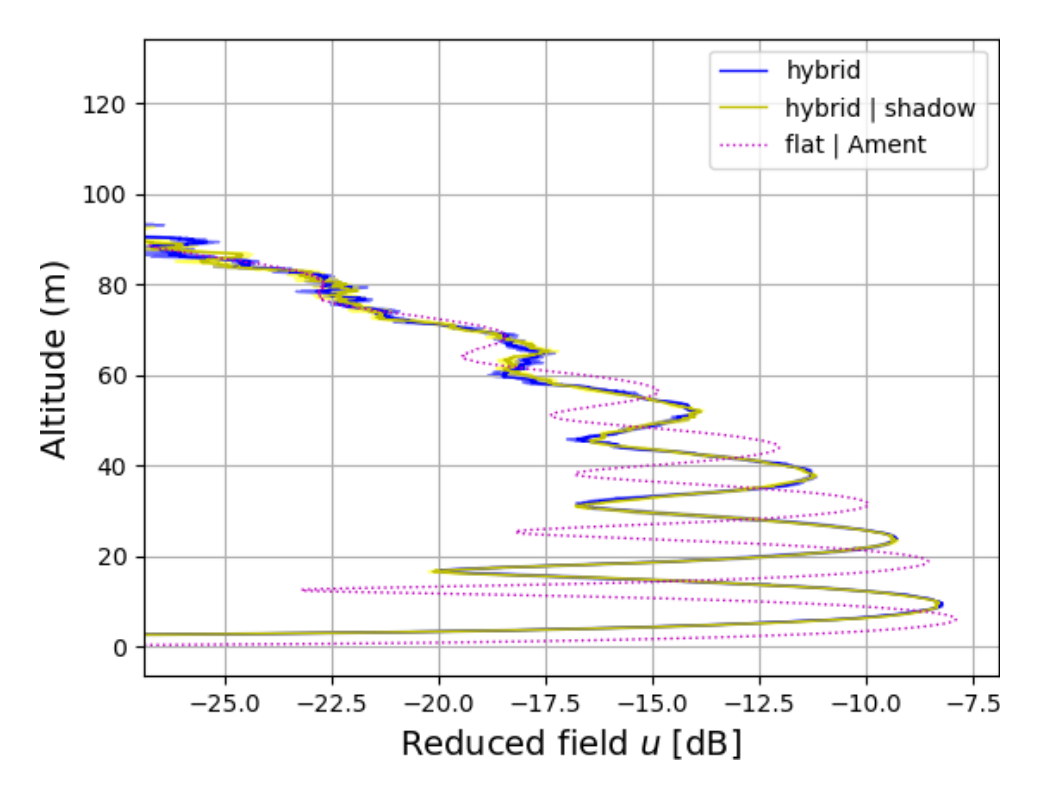


Fig. 1. u (dB) computed at $x = x_{\text{max}}$ for the different approaches.

The shadowing effect of waves is evident as both hybrid methods' positions and extrema values differ from those with a flat sea, consistent with the literature [10], [20]. Additionally, the effect of the sea waves can also be seen since the field curves are less smooth when they are accounted for, as expected. Finally, using a shadowed roughness coefficient for capillary waves shows a slight difference in extrema values, as expected. Thus, from now on this coefficient will be used to account for all phenomena due to sea waves.

B. A fully polluted sea surface

We now consider the fully polluted case with $U_{10}=7$ m/s and two pollutants: one with $E_0=9$ mN/m and $\omega_{\rm po}=6$ rad/s, and the second with $E_0=25$ mN/m and $\omega_{\rm po}=11$ rad/s [23].

To observe the pollutant's impact on propagation and position ourselves in a detection strategy, the field is computed at x_{max} where measurements are performed. As before, in Fig. 2, we provide each case's mean value and 99% CI.

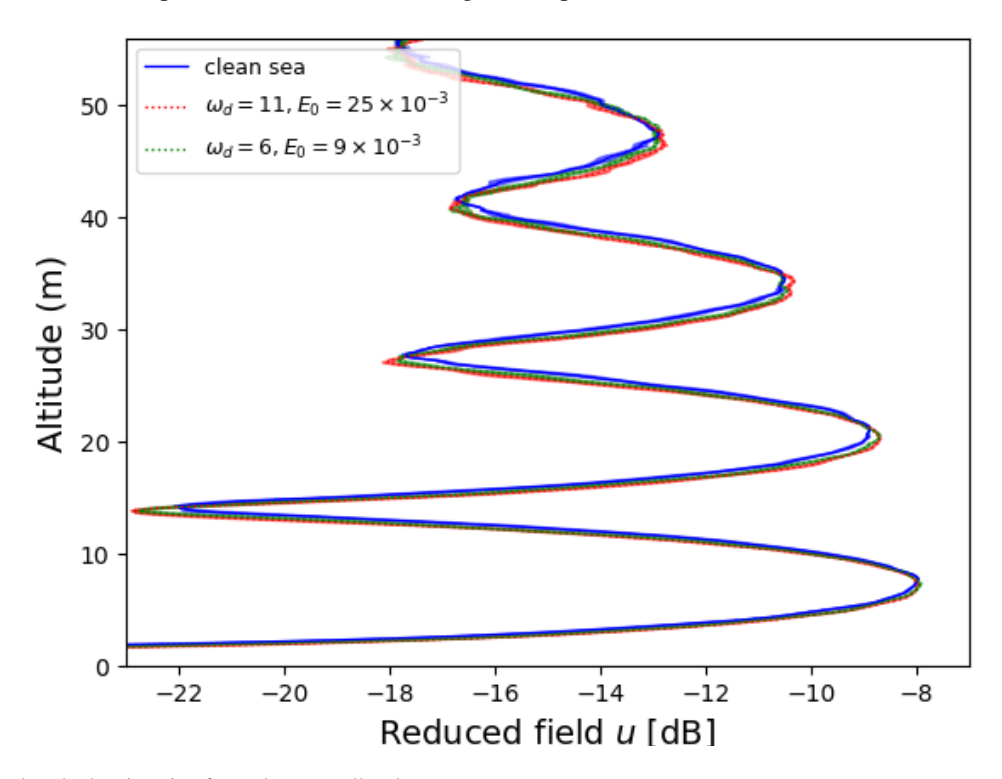


Fig. 2. Field computed at the last iteration for a clean or polluted sea.

In Fig. 2, one can see that the extrema are different when an oil slick is considered, as expected and in line with [10]. Therefore, here the detection is feasible.

C. Different ratios of covered area

We test the method when different ratios of the area covered by the pollutant, i.e., $F_{po} \in [0, 1]$, are considered. In particular, the propagation is computed for $F = \{0, 0.1, 0.3, 0.5, 0.7, 1\}$, for different wind speeds. We consider the second pollutant for these tests, i.e., $\omega_{po} = 11$ rad/s and $E_0 = 25$ mN/m.

First, when the wind speed is $U_{10}=3$ m/s, a flat sea, the fields mean values obtained at $x_{\rm max}$ are plotted in Fig. 3, with a zoom on one lobe to have a better look at the differences. The maximum normalized differences between the fields computed for a clean sea state and the polluted ones are shown in Table I.

TABLE I CASE OF $U_{10}=3$ M/s.

F	1	0.7	0.5	0.3	0.1
Difference (dB)	-23.98	-28.3	-28.1	-32.7	-52.6

As expected, when $F \in]0,1[$ the computed fields are between the bound provided by the case of a clean sea, i.e. F=0, and a fully polluted sea surface, i.e. F=1. In addition, detecting a clean sea from a polluted one becomes more difficult when F decreases since the difference becomes tinier. Directly retrieving F does not seem feasible. Indeed, it depends on the state of the sea and also on the position of the oil slick. To analyze in detail the effect of the pollutant on propagation, we

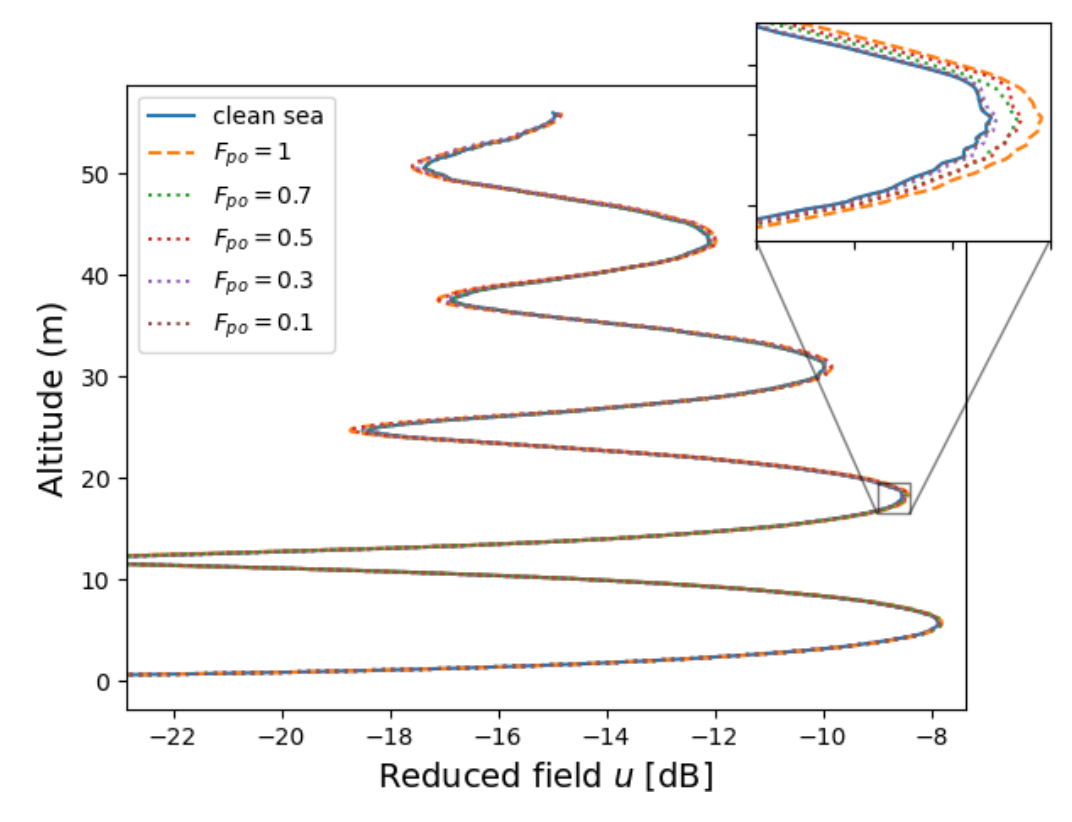


Fig. 3. Fields (u) computed at x_{max} for different F when $U_{10} = 3$ m/s.

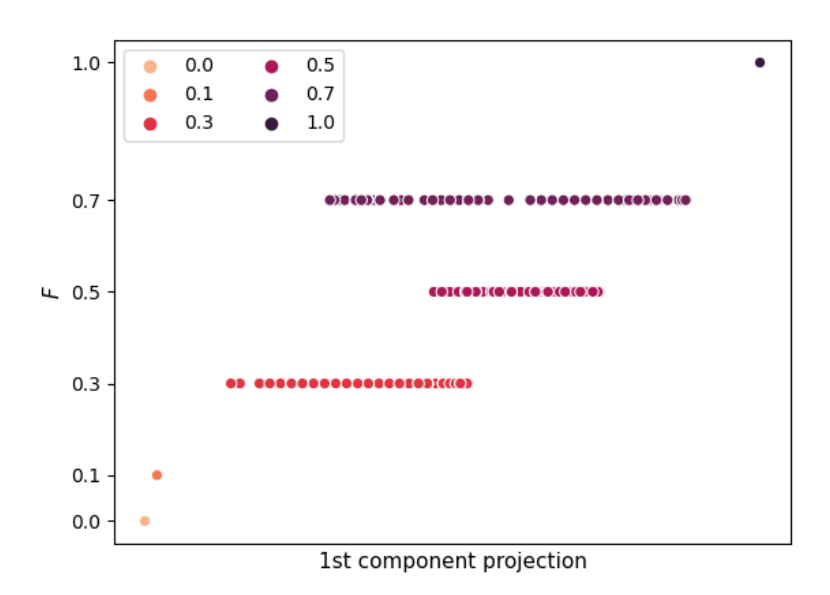


Fig. 4. Samples projection on the 1st SVD component when $U_{10}=3~\mathrm{m/s}$.

created a database of 600 samples of fields, computed for various random sea states and pollutant positions. A singular value decomposition (SVD) applied to this data allowed us to calculate eigenvectors that provide insights into the covered area. In Fig. 4, the projection of our samples on the first eigenvector is shown, with circle colors from pink to black indicating pollutant coverage from 0 to 1.

The first SVD component effectively indicates the extent of sea pollution, from clean to fully polluted. Partially covered cases lie between these extremes, enabling detection when U_{10} is low, even for F=0.1, since F=0 is separated from all the others here. Also, the projection on this axis provides a priori information on F.

Second, we consider a higher wind speed, with $U_{10} = 7$ m/s. In Fig. 5, as before, the field computed at x_{max} when $F = \{0, 0.1, 0.3, 0.5, 0.7, 1\}$ are plotted, with the same zoom. Also, Table II shows the maximum normalized differences between the fields for clean and polluted sea states. For comparison the maximum normalized difference for two different

clean sea states (two surface generations) is of order -23 dB.

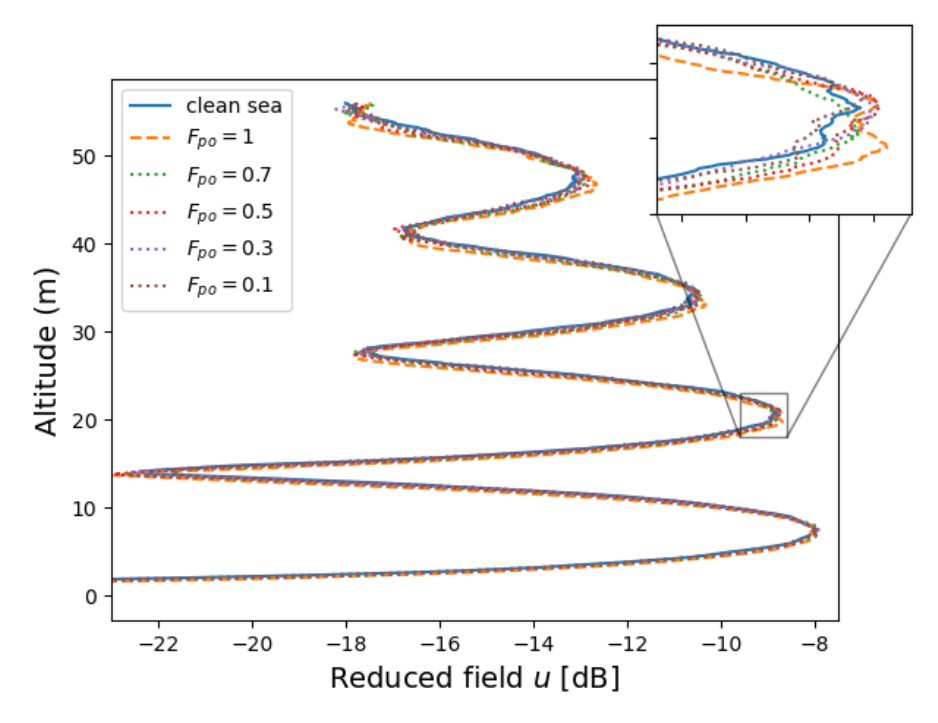


Fig. 5. Fields (u) computed at x_{max} for different F when $U_{10} = 7$ m/s.

TABLE II CASE OF $U_{10} = 7$ M/s.

Г	1	0.7	0.5	0.0	0.1
F	1	0.7	0.5	0.3	0.1
Difference (dB)	-12.7	-15.8	-17.3	-19.4	-20.1

The conclusion remains consistent: F = 0 and F = 1 bound the other cases. However, for F = 0.3, the field's similarity to a clean or fully polluted sea depends on the oil slick's position, i.e. the polluted area affected by the electromagnetic field.

To further explore detection feasibility, we constructed a database of 600 samples of virtual field measurements and applied a SVD. The projection of these samples on the first component is shown in Fig. 6.

As before, the first axis of the SVD indicates the proximity of a sample to a clean or fully polluted one. Until F=0.5 detection is feasible using this projection since these cases are separated from F=0, but F seems intractable.

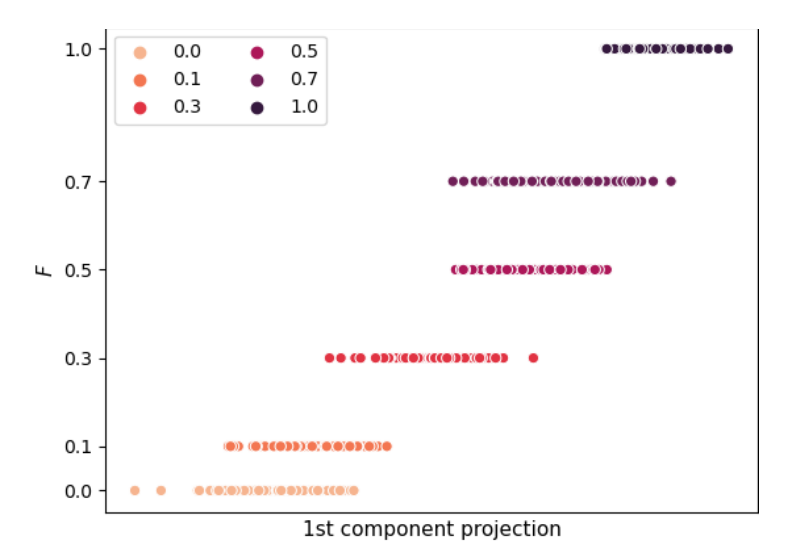


Fig. 6. Samples projection on the 1st SVD component when $U_{10}=7\,\mathrm{m/s}.$

V. CONCLUSIONS

We presented a shadowed hybrid model for computing the propagation of electromagnetic waves over a sea surface partially or fully covered with an insoluble pollutant.

In particular, by introducing the shadowed roughness coefficient, we improve the hybrid method [11] to account for a sea surface. We also build on the existing damp model, which introduces the effect of an oil slick on the sea surface. Nonetheless, we do not restrict ourselves to fully covered sea surfaces, and the ratio of the covered area is accounted for as a random process. The method has been evaluated in different cases, and compared with the results obtained in the literature, showing promising results. Also, a first statistical analysis through SVD has been proposed.

Our study opens up several interesting perspectives for future research. We are currently working on building a representative dataset of virtual experiments of our model and improving the statistical analysis we began here. Another direction is to extend the model to consider insoluble pollutants that form an emulsion of oil and water at higher wind speeds, and to study the case of composite medium [9]. Finally, the generalization to 3D is currently under study.

REFERENCES

- [1] P. P. Lombardini, B. Fiscella, P. Trivero, C. Cappa, and W. Garrett, "Modulation of the spectra of short gravity waves by sea surface films: slick detection and characterization with a microwave probe," *Journal of Atmospheric and Oceanic Technology*, vol. 6, no. 6, pp. 882–890, 1989.
- [2] N. Skou, "Microwave radiometry for oil pollution monitoring, measurements, and systems," *IEEE Transactions on Geoscience and Remote Sensing*, no. 3, pp. 360–367, 1986.
- [3] G. Franceschetti, A. Iodice, D. Riccio, G. Ruello, and R. Siviero, "SAR raw signal simulation of oil slicks in ocean environments," *IEEE Transactions on Geoscience and Remote Sensing*, vol. 40, no. 9, pp. 1935–1949, 2002.
- [4] S. Angelliaume, P. C. Dubois-Fernandez, C. E. Jones, B. Holt, B. Minchew, E. Amri, and V. Miegebielle, "SAR imagery for detecting sea surface slicks: Performance assessment of polarization-dependent parameters," *IEEE Transactions on Geoscience and Remote Sensing*, vol. 56, no. 8, pp. 4237–4257, 2018.
- [5] N. Pinel, N. Déchamps, and C. Bourlier, "Modeling of the bistatic electromagnetic scattering from sea surfaces covered in oil for microwave applications," *IEEE Transactions on Geoscience and Remote Sensing*, vol. 46, no. 2, pp. 385–392, 2008.
- [6] C.-S. Yang, S.-M. Park, Y. Oh, and K. Ouchi, "An analysis of the radar backscatter from oil-covered sea surfaces using moment method and Monte-Carlo simulation: Preliminary results," Acta Oceanologica Sinica, vol. 32, no. 1, pp. 59–67, 2013.
- [7] H. Zheng, J. Zhang, A. Khenchaf, and X.-M. Li, "Study on non-Bragg microwave backscattering from sea surface covered with and without oil film at moderate incidence angles," *Remote Sensing*, vol. 13, no. 13, p. 2443, 2021.
- [8] T. Elfouhaily, B. Chapron, K. Katsaros, and D. Vandemark, "A unified directional spectrum for long and short wind-driven waves," *Journal of Geophysical Research: Oceans*, vol. 102, no. C7, pp. 15781–15796, 1997.
- [9] T. Meng, K.-S. Chen, X. Yang, F. Nunziata, D. Xie, and A. Buono, "Simulation and analysis of bistatic radar scattering from oil-covered sea surface," *IEEE Transactions on Geoscience and Remote Sensing*, vol. 60, pp. 1–15, 2021.
- [10] N. Pinel, C. Bourlier, and J. Saillard, "Forward radar propagation over oil slicks on sea surfaces using the ament model with shadowing effect," *Progress In Electromagnetics Research*, vol. 76, pp. 95–126, 2007.
- [11] O. Benhmammouch, A. Khenchaf, and N. Caouren, "Modelling roughness effects on propagation of electromagnetic waves in a maritime environment: A hybrid approach," *IET radar, sonar & navigation*, vol. 5, no. 9, pp. 1018–1025, 2011.
- [12] T. Bonnafont, O. Benhmammouch, and A. Khenchaf, "A two-way split-step wavelet scheme for tropospheric long-range propagation in various environments," *Remote Sensing*, vol. 14, no. 11, p. 2686, 2022.
- [13] M. Levy, Parabolic equation methods for electromagnetic wave propagation. No. 45, IET, 2000.
- [14] T. Meng, F. Nunziata, A. Buono, X. Yang, and M. Migliaccio, "On the joint use of scattering and damping models to predict x-band co-polarized backscattering from a slick-covered sea surface," *Frontiers in Marine Science*, vol. 9, p. 1113068, 2022.
- [15] H. Jafarzadeh, M. Mahdianpari, S. Homayouni, F. Mohammadimanesh, and M. Dabboor, "Oil spill detection from synthetic aperture radar earth observations: A meta-analysis and comprehensive review," GIScience & Remote Sensing, vol. 58, no. 7, pp. 1022–1051, 2021.
- [16] T. Bonnafont, R. Douvenot, and A. Chabory, "A local split-step wavelet method for the long range propagation simulation in 2D," *Radio Science*, vol. 56, no. 2, pp. 1–11, 2021.
- [17] H. Zhou, R. Douvenot, and A. Chabory, "Modeling the long-range wave propagation by a split-step wavelet method," *Journal of Computational Physics*, vol. 402, p. 109042, 2020.
- [18] W. Ament, "Toward a theory of reflection by a rough surface," Proceedings of the IRE, vol. 41, no. 1, pp. 142-146, 1953.
- [19] A. Miller, R. Brown, and E. Vegh, "New derivation for the rough-surface reflection coefficient and for the distribution of sea-wave elevations," in *IEE Proceedings H-Microwaves, Optics and Antennas*, pp. 114–116, 1984.
- [20] V. Fabbro, C. Bourlier, and P. Combes, "Forward propagation modeling above gaussian rough surfaces by the parabolic shadowing effect," *Progress In Electromagnetics Research*, vol. 58, pp. 243–269, 2006.
- [21] X.-M. Guo, Q.-L. Li, Q. Zhao, S.-F. Kang, Y.-W. Wei, and L.-X. Yang, "A comparative study of rough sea surface and evaporation duct models on radio wave propagation," *IEEE Transactions on Antennas and Propagation*, 2023.
- [22] G. A. Deschamps, "Gaussian beam as a bundle of complex rays," Electronics letters, vol. 7, no. 23, pp. 684-685, 1971.
- [23] T. Friisø, Y. Schildberg, O. Rambeau, T. Tjomsland, H. Førdedal, and J. Sjøblom, "Complex permittivity of crude oils and solutions of heavy crude oil fractions," *Journal of Dispersion Science and Technology*, vol. 19, no. 1, pp. 93–126, 1998.